Geomechanics and Engineering, *Vol. 35, No. 2 (2023) 209-219*
https://doi.org/10.12989/gae.2023.35.2.209

Numerical investigation into particle crushing effects on the shear behavior of gravel

Xi Li*[1,2,3], Yayan Liu[2], Guoping Qian**[1,2], Xueqing Liu[4], Hao Wang[3] and Guoqing Yin[3]

[1]*National Engineering Research Center of Highway Maintenance Technology, Changsha University of Science and Technology, Changsha, Hunan 410114, China*
[2]*School of Traffic and Transportation Engineering, Changsha University of Science and Technology, Changsha, Hunan 410114, China*
[3]*Ecole des Ponts ParisTech, Laboratoire Navier/CERMES, 6 et 8 avenue Blaise Pascal, 77455 Marne La Vallée cedex 2, France*
[4]*Shanghai Zhuxin Real Estate Broker Co., Ltd., Shanghai 201418, China*

(*Received December 2, 2022, Revised October 4, 2023, Accepted October 5, 2023*)

Abstract. This paper presents numerical investigations into the particle crushing effect on the shear properties of gravel under direct shear condition. A novel particle crushing model was developed based on the octahedral shear stress criterion and fragment replacement method. A series of direct shear tests were carried out on unbreakable particles and breakable particles with different strengths. The evolutions of the particle crushing, shear strength, volumetric strain behavior, and contact force fabric during shearing were analyzed. It was observed that the number of crushed particles increased with the increase of the shear displacement and axial pressure and decreased with the particle strength increasing. Moreover, the shear strength and volume dilatancy were obviously decreased with particle crushing. The shear displacement of particles starting to crush was close to that corresponding to the peak shear stress got. Besides, the shear-hardening behavior was obviously affected by the number of crushed particles. A microanalysis showed that due to particle crushing, the contact forces and anisotropy decreased. The mechanism of the particle crushing effect on the shear strength was further clarified in terms of the particle friction and interlock.

Keywords: granular materials; ground improvement; numerical analyses; rock fills; shear strength

1. Introduction

Gravels are widely used as foundation fillers for airports, highways, and earth-rock dams due to their easy availability, high strength, and good permeability (Sukkarak *et al*.2021, Tu *et al*. 2022, Gong *et al*. 2021, Ma *et al*. 2021). However, the gravel particles may crush under multiple factor effects of suffered stress and strength deterioration (Armaghani *et al*. 2020, Wang *et al*. 2022, Xiao *et al*. 2021). As a result of particle crushing, the particle size distribution and fabric properties change, which in turn affects the shear properties of the foundations (Ueng and Chen 2000, Yu 2017). Considering that shear strength is the main factor contributing to the instability and failure of the filled foundations (Thay *et al*. 2013, Mase *et al*.2019, Sukkarak *et al*. 2021, VandenBerge *et al*. 2021, Xiao *et al*. 2020, Kumar *et al*. 2021, Shi *et al*. 2020), it is of great significance to investigate the effect of particle crushing on the shear properties of gravels for improving the long service of civil engineering.

Many experiments including indoor or on-site direct shear tests have been carried out to study the effect of particle crushing on the shear properties of gravels (Ueng and Chen 2000, Yu 2017, Chen *et al*. 2018, Wei *et al*. 2021). Ueng and Chen (2000) reported that the effect of particle crushing on the shear strength of sand could be correlated with the rate of energy consumption. Yu (2017) and Chen *et al*. (2018) further found that particle crushing had a significant influence on friction-dilatancy behavior, while Wei *et al.* (2021) emphasized that under shear deformation, particle rearrangements could increase the shear strength of calcareous sands with the crushing decreasing. However, these physical tests have obvious drawbacks that the particle crushing can't be controlled. The particle crushing and shear properties keep changing all the time during the test. It's harder to carry out a comparative analysis of particles under the same physical structure in the presence or absence of particle crushing.

In recent decades, the discrete element method (DEM) has been widely adopted to investigate the influence of particle crushing. There are mainly includes two methods: the bonded-particle method (Xu and Xu 2021, Indraratna *et al*. 2010, Yang *et al*. 2022) and the fragment replacement method (Tavares and Chagas 2021, LI Xi *et al*. 2020, Liu *et al*. 2021). The former implies that several small bonded particles are bonded together to simulate a large particle, and unbonded after crushing. This method earns priority in simulating the complex particle's morphology. However, its computational efficiency will decrease when too many particles are involved. In contrast, for the fragment replacement method, the crushed particles are replaced with several small child particles when a particle is crushed, which is more efficient for the case with a large number of

*Corresponding author, Associate Professor
E-mail: lixi@csust.edu.cn
**Corresponding author, Professor
E-mail: guopingqian@csust.edu.cn

ISSN: 2005-307X (Print), 2092-6219 (Online)

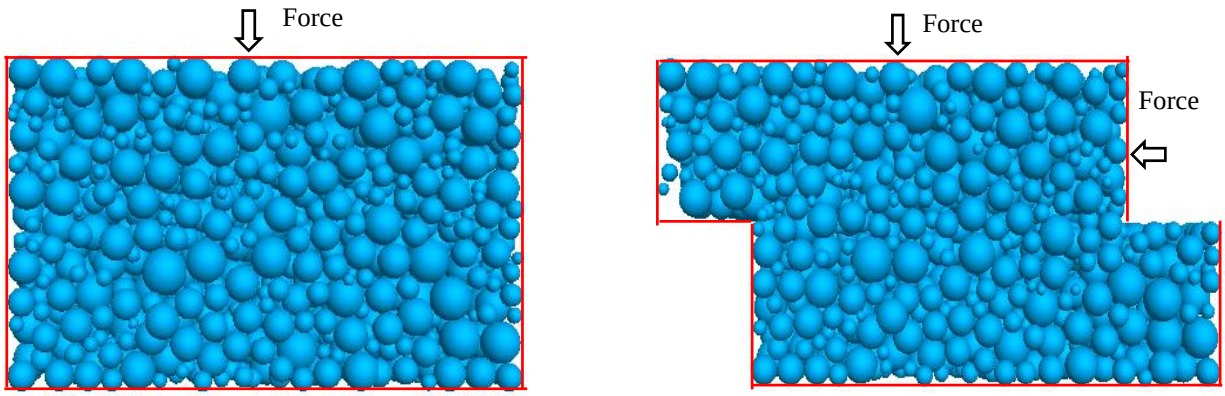

(a) before shearing (b) after being sheared

Fig. 1 The numerical model of direct test

particles (LI Xi *et al*. 2020, Liu *et al*. 2021). Indraratna *et al*. (2010) presented the evolution of micromechanical parameters to explain the mechanism of particle crushing using DEM. Xu and Xu (2021) used PFC2D (Particle Flow Code in 2 Dimensions) to simulate rock particle crushing. However, few studies have explored the effect of particle strength on shear properties.

To simulate particle crushing using DEM, the key point in the fragment replacement method is to determine the particle crushing criteria. Some studies have been carried out on this topic. Typically, Lobo-Guerrero and Vallejo (2006) established a two-dimensional particle crushing model based on the coordination number less than three. Russell and Wood (2009) proposed a maximum shear strength theory based on the particle radial crushing test. Subsequently, Russell and Wood (2009) proved that the theory was applicable in the cases of coordination numbers between 6 and 12. It can be seen that the existing particle crushing criteria seldom take into account the change of the coordination number in the shearing process. Therefore, there is still a lack of thorough understanding of the influence of particle crushing on shear behavior.

In this study, a novel particle crushing criterion based on octahedral shear stress was proposed. Correspondingly, a particle crushing model was developed based on the PFC3D (Particle Flow Code in 3 Dimensions). A series of numerical direct shear tests with different axial loads and particle strengths was carried out. The distribution and the number of crushed particles were analyzed. Combining with the multiscale analyses on the shear strength, residual strength, volume change, and contact-force-fabric, enabling to clarifying the mechanism of the effect of particle crushing on the shear behaviors of gravels.

2. Methodology of modeling

2.1 Development of shear tests

In this study, a DEM model of direct shear tests was established using the Particle Flow Code in 3D (PFC3D). As shown in Fig. 1, the model includes two kinds of elements: walls and particles. The walls play the role of the cube boundary, which can be moved to shear the particles inside. The particles inside the boundary played the role of the gravel being sheared. The gravel's mechanical behaviour could be depicted by the movement of each particle with the contact forces. The mechanical contact model determining the contact force between particles and particles-walls is a crucial issue that is carefully assessed as follows.

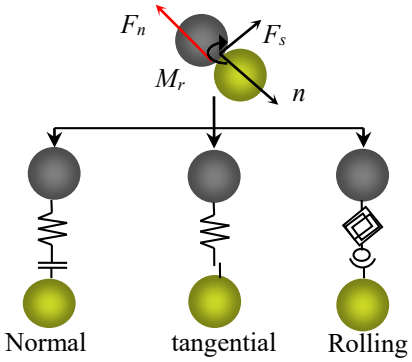

Fig. 2 Schematic diagram of rolling resistance contact model

2.1.1 Contact model and parameters determination

In the PFC model, the interaction between particles is determined by the contact model. The direct shear test often results in particle flipping, posing challenges for simulating surface roughness and torque transfer using the commonly employed Hertz model in PFC. Moreover, it is crucial to consider the significant influence of rolling resistance on particle shear behavior. To overcome this problem, The rolling resistance contact model (Cundall 1988), which includes the normal contact, tangential contact, and rotational moment (Fig. 2) is adopted in this model. The influence of the particle morphology and surface friction on the shear behavior is taken into consideration with the parameters of rolling resistance. To determine the value of the parameters in the hysteretic model (Table 1), the relative reports were collected and analyzed carefully (Lobo-Guerrero and Vallejo 2006, Russell and Wood 2009, Cundall 1988, SHEN *et al*. 2019, ZHANG *et al*. 2018). And the comparison with other research methods is essential in the selection of shear strength (Surarak *et al*.

Size of up shear box	50 × 50 × 15cm^3
Size of below shear box	50 × 50 × 15cm^3
Shear velocity	1.0mm/s
Shear displacement	50mm

Fig. 3 Large direct shear apparatus and set up

Table 1 Parameters of DEM simulations

Parameters	symbol	value
Normal stiffness	k_n	5.5×10^8
Shear stiffness	k_s	5.5×10^8
Sample width	D/mm	88
Sample height	H/mm	56
Initial porosity	n/%	45.5
Young's modulus	E/Pa	2.6×10^9
Weibull modulus	m	3.3
Particle diameter	d/mm	5.0
Limit diameter	d_{limit}/mm	1.0
Particle true density	ρ_s/(g/cm^3)	2.65
Rolling friction coefficient	rrf	0.1
Weibull strength	wellstr	37.5
Shear velocity	v(mm/s)	0.02

2012, Likitlersuang, *et al*. 2013, Likitlersuang *et al*. 2018). Additionally, a series of large-scale shear tests for granite was conducted to check the reliability of the developed model (Fig. 3).

2.1.2 Sample design and reliability check

To verify the model reliability, a series of indoor large-scale direct shear tests were carried out with granite (Fig. 3). The shear device is controlled with a servo control system, enabling shear the granite sample under design axial pressure and shear rate. The upper and lower shear boxes were both 500×500×150 mm^3. The test material was weakly weathered granite with a relative density of 2.68 and a compressive strength of 100 MPa. The numerical model incorporated particles of continuously varying sizes, and particle gradation was generated based on a Gaussian distribution between partitions. The particle size distribution is shown in Fig. 4 with a maximum particle size of 45 mm. The porosity of the specimen was 0.46. During the shear test, the upper shear box moved at a rate of 1 mm/min, while the lower shear box was fixed. The total shear displacement was 50 mm (10% of the length of the specimen). Direct shear tests were conducted at axial pressures of 100 kPa, 200 kPa, and 300 kPa, respectively. The shear displacement and shear stress during each test were detected for analysis.

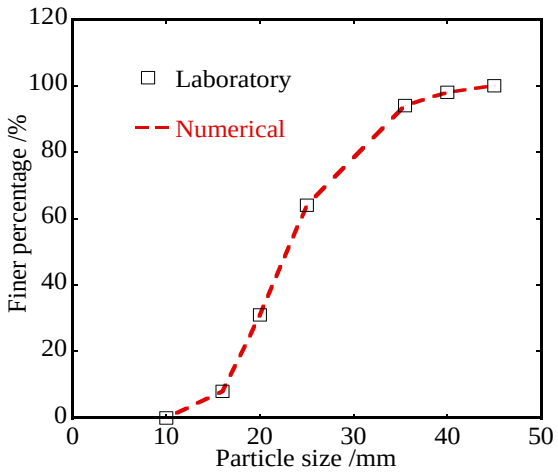

Fig. 4 Particle size distribution of the granite

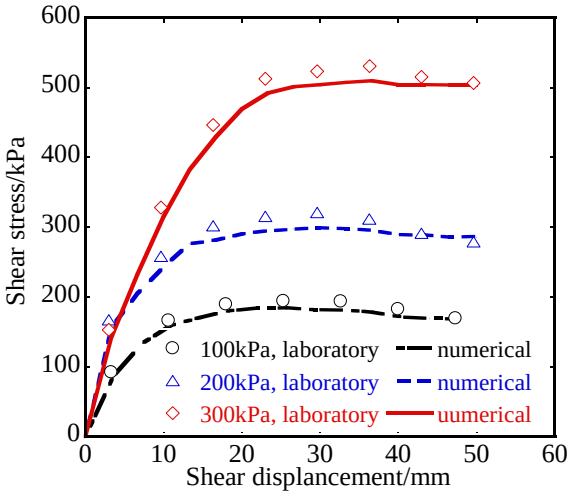

Fig. 5 Comparison of shear test between laboratory and numerical

In the numerical model, key factors including particle size distribution, initial porosity, specimen size, and loading conditions were identical to those of the indoor tests. To obtain a specimen with a uniform initial porosity, a specific number of particles was generated in a large space based on the target porosity. Then a vertical force was applied until the specimen was compressed to a specified height. The vertical force remained constant for a sufficient time step until the unbalanced force ratio was less than 10^{-5}. The loading conditions for the numerical tests are identical to those used in the indoor shear experiments. The results are shown in Fig. 5.

It can be seen from Fig. 5 that under the three axial pressures, the shear displacement-shear stress curve obtained with the indoor was very close to that of the numerical results. Specifically, under the same axial pressure, the shear stress gradually increased and then decreased with the increase of the shear displacement. Comparing different axial pressure conditions, the greater the axial pressure was, the larger the peak shear stress was.

2.2 Particle crushing model

The fragment replacement method is adopted in this study for its advantages in computational efficiency. Two key issues are involved in this method, which are the particle crushing criteria and the crushing pattern of the child particles.

2.2.1 Particle crushing criteria

Particle crushing criteria is the thresholding for particle crushing. Currently, there are mainly two crushing criteria. One is the maximum force criterion (Ben and Einav 2008), which uses the tensor of the equivalent force as the criterion. The other is the maximum stress criterion. For instance, Zhou *et al*. (2016) employed the Mohr-Coulomb criterion with a tension cut-off as the particle crushing criterion. McDowell and de Bono (2003, 2012) pointed out that particle crushing was determined by compressive stress rather than by tensile stress. Given the fact that there are often multiple contact points between particles, it is suitable to use the octahedral shear stress criterion in this study

$$q = \frac{1}{3}\left[(\sigma_1 - \sigma_2)^2 + (\sigma_2 - \sigma_3)^2 + (\sigma_1 - \sigma_3)^2\right]^{1/2} \quad (1)$$

where, σ_1, σ_2, and σ_3 are the principal stresses of the particles.

For the PFC, the particles loop command was used to obtain the stress tensors of each particle and thereby calculate the octahedral shear stress q. To determine whether a particle breaks, it is necessary to compare the calculated q with the particle strength. Hence, the true strength of the particles is needed. Considering the natural defects inside, the larger particles are easier to crush (Mcdowell *et al*. 2013, McDowell and Humphreys 2002). Moreover, the strength may vary between particles with the same size. De Bono and Mcdowell (2014) used a Weibull distribution to describe the strength of quartz sand $q_{\lim}$, and a scale factor was introduced to describe the characteristic:

$$q_{lim} = q_0 f(d) \quad (2)$$

where q_0 is the characteristic strength of the particles, which corresponds to the strength when 37% of the particles are not broken. The scale factor is expressed as

$$f(d) = \left(\frac{d}{d_0}\right)^{-3/m} \quad (3)$$

where m is the Weibull modulus, m = 3.3 for coarse-grained soil. d_0 is the reference diameter, which was set to 3.0 mm (De Bono and Mcdowell 2014).

During the direct shear tests, the values of q and $q_{\lim}$ are monitored in real-time. Once the shear stress reaches the crushing criteria (i.e., $q \geq q_{\lim}$), the particles are broken, and the crushing pattern of the child particles is initiated.

2.2.2 Crushing pattern of the child particles

The crushing pattern of the child particles includes three key issues: the number of child particles, the distribution of the child particles, and the conservation of particle mass before and after crushing. Regarding the number of child particles, Takei *et al*. (2001) reported that the number of child particles in natural quartz sand was generally less than 10. As shown in Fig. 6, combined with the computational efficiency of the model, the number of child particles was set to four in this study.

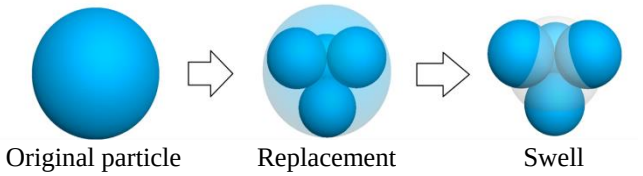

Fig. 6 Numerical model of a particle crushes

In terms of the distribution of child particles, Li *et al*. (2019) established a crushing pattern for child particles based on the Apollonian sphere packing (Borkovec *et al*. 1994). Specifically, four child particles that were circumscribed to each other were first generated in the parent sphere, and at the same time, the child particles were inscribed with the parent sphere. The fractal dimension of the model was 2.47 (Borkovec *et al*. 1994), which was very close to the fractal dimension of actual gravels in the ultimate breakage state (i.e., 2.50).

To ensure the mass conservation of the particles after crushing, Ben-Nun and Einav (2009) proposed the linear expansion method, and Zhang *et al*. (2017) expanded the method to three dimensions and verified the applicability of the linear expansion method through compression experiments. In this study, the broken parent particle was replaced with four circumscribed within the parent particle area. Then, according to the total volume conservation, the child particles were linearly expanded. Considering the calculation efficiency, a limit crushing diameter $d_{\lim}$ was introduced, which meant particles were smaller, and no further crushing occurred (Ciantia *et al*. 2015). The value of $d_{\lim}$ was equal to 1/4 the average particle diameter in this study.

2.3 Set up of shear tests

As shown in Fig. 7, the dimensions of the shear box were 88×88×56 mm. The initial diameter of the particles was the same, 5.0 mm (i.e., less than 1/10 of the specimen). The shear speed was 0.02 mm/s and the termination condition was a total shear displacement of 17.6 mm (20% of the width of the shearing box). To compare the effect of particle crushing on the shear properties, the shear tests were divided into six groups. In group 1, there was no particle crushing during the shear test. In the other five groups, the particle crushing code was introduced, and the characteristic strength q_0 was adjusted to characterize particles with different strengths. The values of q_0 were thus set to 3.0 MPa, 3.75 MPa, 4.5 MPa, 5.0 MPa, and 5.5 MPa in each group, respectively. The initial conditions and loading methods were the same and the particle crushing was the only independent variable. Direct shear tests were then carried out under axial pressures of 150 kPa, 200 kPa, 250 kPa, and 300 kPa. The particle crushing status, shear

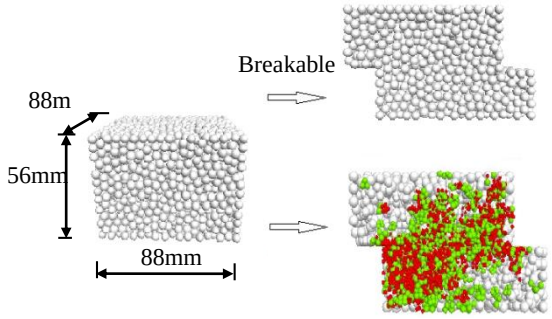

Fig. 7 Numerical model of direct shear test (Grey indicates no broken particles, green indicates primary fragmentation and red indicates secondary fragmentation)

stress-displacement relationship, volumetric shear characteristics, and particle contact force fabric were detected.

3. Results

3.1 Particle crushing evolution

Fig. 8 shows the distribution of particles after the shear test in group six with q_0=5.5 MPa. It can be observed that the number of crushed particles increased with the axial stress. Besides, particle crushing was mainly along the diagonal of the shear box. When the axial pressure was 150 kPa, particle crushing first appeared at the ends of the diagonal (Fig. 8(a)). Under the axial stress of 200 kPa, the number of crushed particles increased, and these crushed particles were mainly located along the diagonal line and the shear surface (Fig. 8(b)). When the axial stress increased to 250 kPa and 300 kPa, the number of crushed particles further increased, and the range of particle crushing extended to the entire specimen (Figs. 8(c) and 8(d)).

Fig. 9 depicts the number of particles in different sizes. After shearing under the same axial stress, the larger value

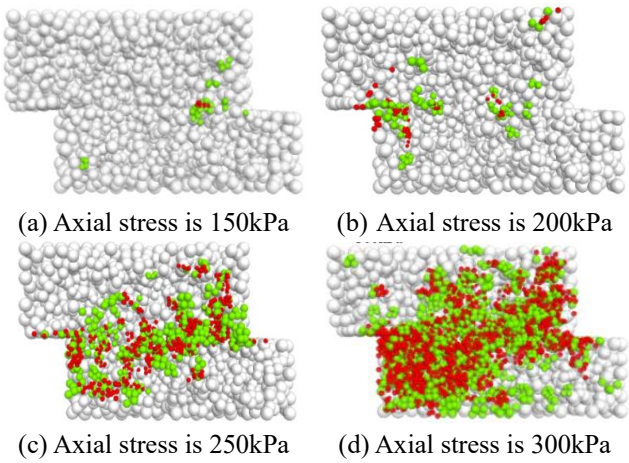

(a) Axial stress is 150kPa (b) Axial stress is 200kPa

(c) Axial stress is 250kPa (d) Axial stress is 300kPa

Fig. 8 Particle breakage after direct shear tests

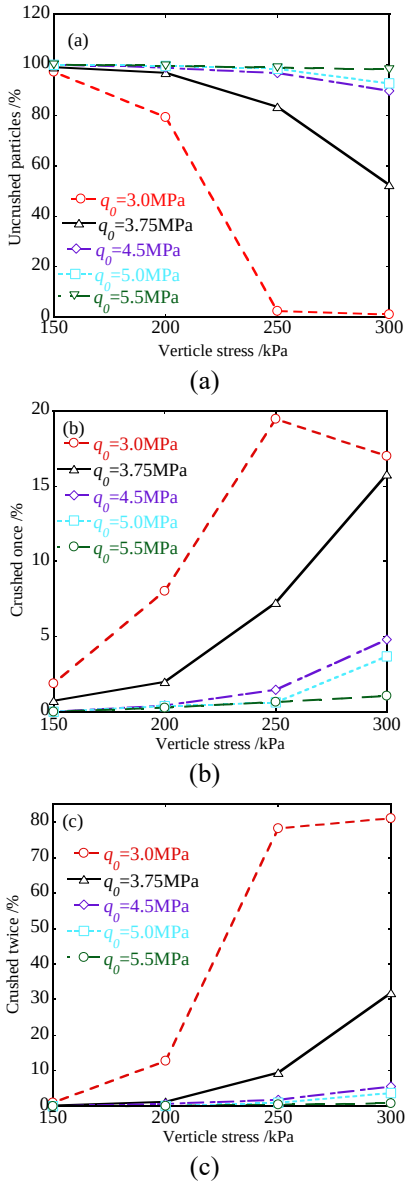

Fig. 9 The number of crushed particles after direct shear test

of q_0 was, the smaller number of particles crushed. When q_0 was larger than 4.5 MPa, more than 90% of the particles were uncrushed. While q_0 was equal to 3.0 MPa, almost all the particles were crushed when shearing under an axial pressure of 250 kPa. Besides, approximately 20% of the particles were crushed twice in this case. When sheared under the axial stress was 300 kPa, the number of particles that underwent secondary crushing increased.

3.2 Displacement-shear stress and strength

Fig. 10 shows the shear stress-shear displacement curve derived from different cases. These curves shared some in common that, for a certain axial stress shearing, the curves overlapped in the early stage of shearing, and then separated. This separation point implied particles began to crush. Besides, the smaller the characteristic strength was, the earlier the separation point was observed, and the smaller the peak strength was. Noticeably, there was not

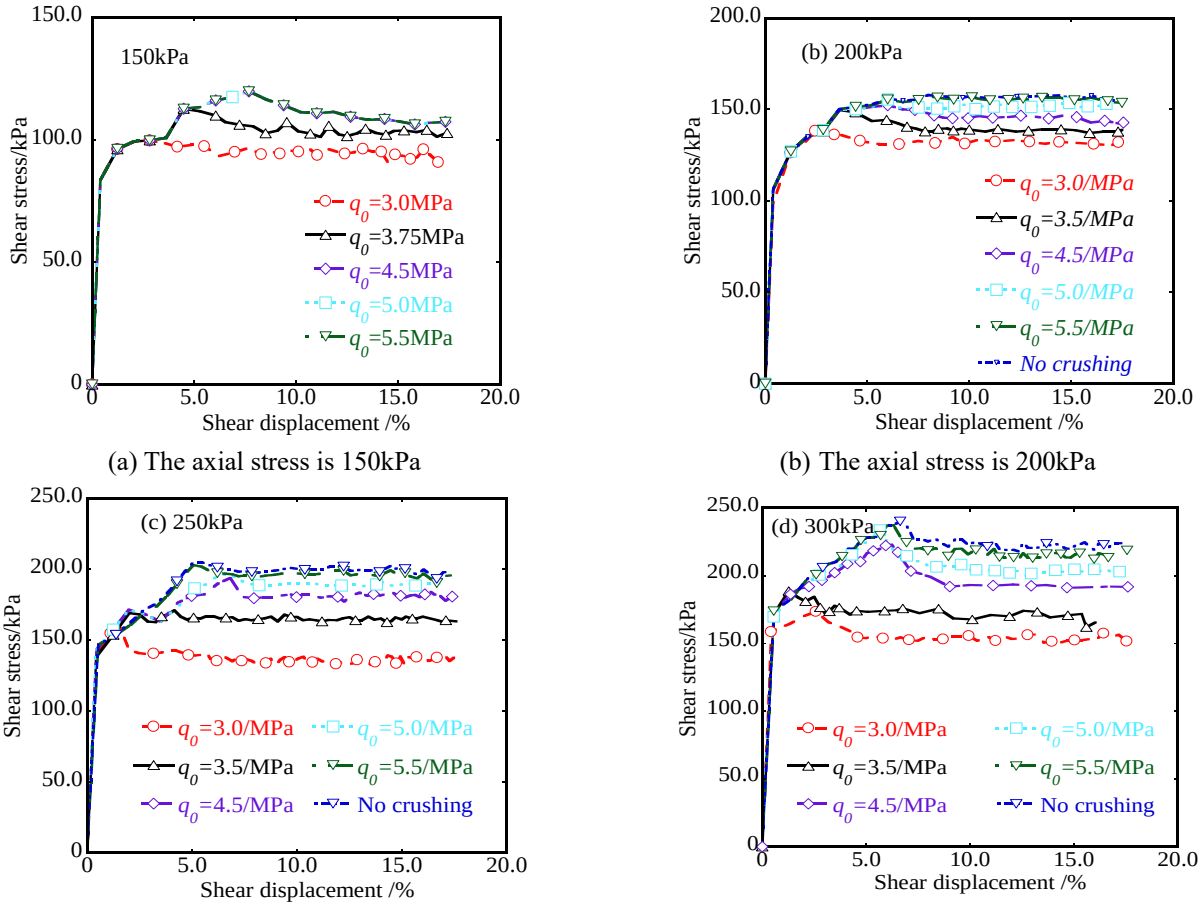

(a) The axial stress is 150kPa

(b) The axial stress is 200kPa

(c) The axial stress is 250kPa

(d) The axial stress is 300kPa

Fig. 10 Shear stress against shear displacement

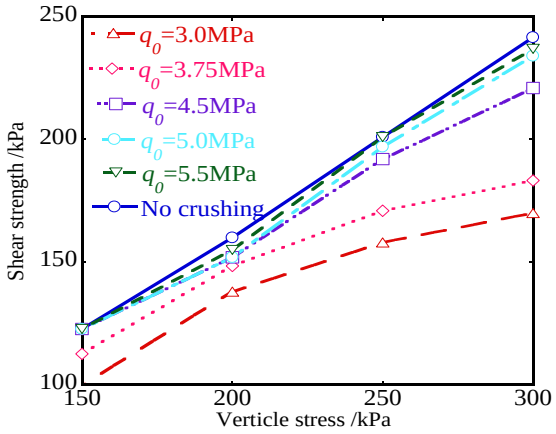

Fig. 11 Shear strength of particles with different characteristic strength

necessarily an obvious peak shear stress appeared during the shear test for particles with different characteristic strengths. However, the shear displacement at particle crushing was close to the shear displacement at the peak shear stress. This is because particle crushing weakened the particles' skeleton, and the shear resistance was reduced.

Compared with the curves derived from shearing tests under different axial stress conditions, the shear displacement at particles started to crush decreased as the axial stress increased, and the overlapping part of the shear curves was reduced.

3.3 Internal friction angle

To investigate the influence of particle crushing on the shear strength, the strength envelopes of particles with different characteristic strength are plotted, as shown in Fig. 11. When particles were unable to crush, the strength envelope showed as a straight line. For crushable particles, an obvious nonlinear relationship was observed between the axial stress and shear strength, which became more serious for particles with a smaller value of characteristic strength.

3.4 Volumetric strain behavior

Fig. 12 presents the variation of the specimen height during shearing. All the specimens exhibited shear shrinkage, which was partly due to the initial void ratio of the specimen (0.455) being relatively large. Moreover, a larger amount of volumetric shrinkage was observed for specimens with smaller particle characteristic strength. For particles with the same characteristic strength, the larger the axial stress was, the more obvious volumetric shrinkage was. For shearing on the particles with the largest characteristic strength (q_0=5.5 MPa), the specimen height

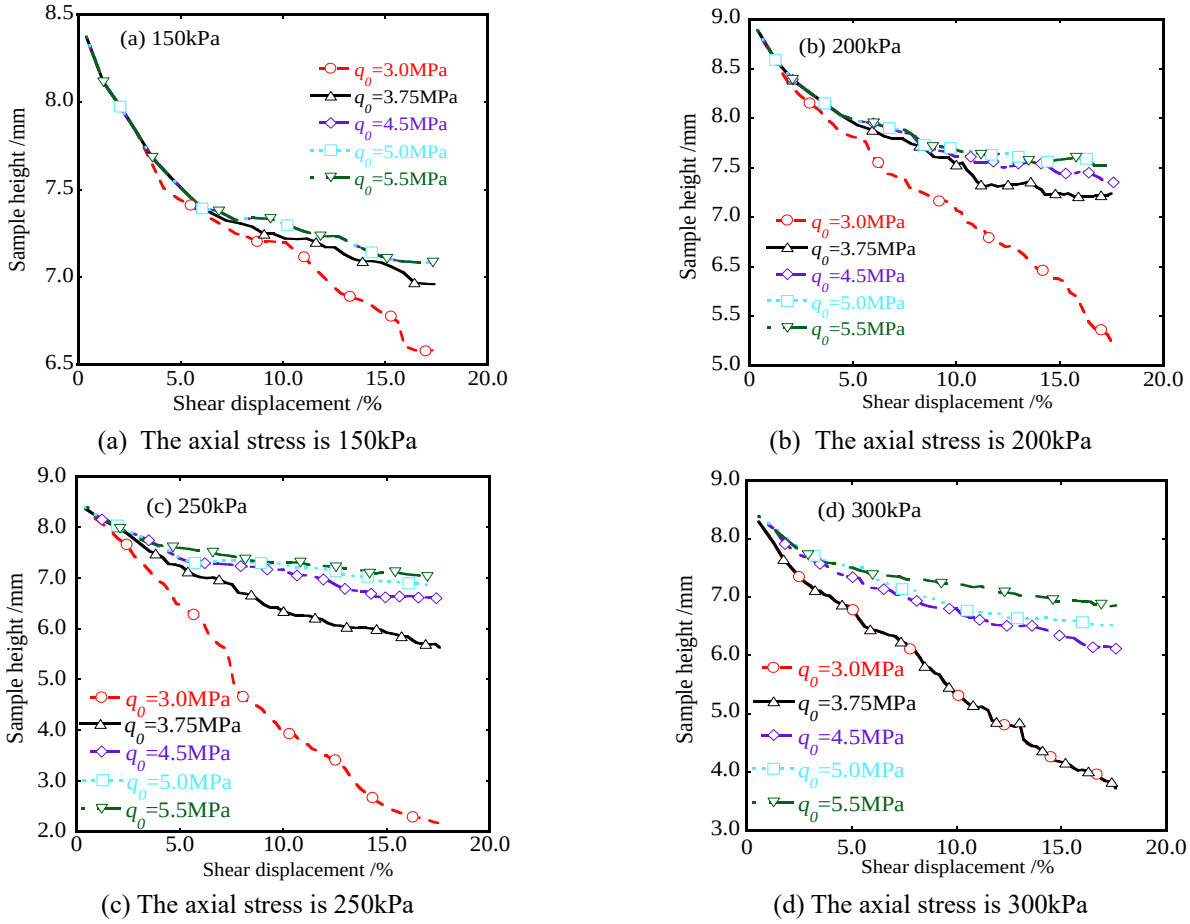

(a) The axial stress is 150kPa

(b) The axial stress is 200kPa

(c) The axial stress is 250kPa

(d) The axial stress is 300kPa

Fig. 12 Sample height against shear displacement

after shearing under different axial stress was similar to 7.2 mm. While, for shearing on the particles with the smallest characteristic strength (q_0=3.0 MPa), the maximum height difference between different tests was 6.5 mm.

3.5 Contact force fabric

During a shear test, the particle contact force fabric is used to describe the particle positions and their interaction. To comprehensively analyze the effect of particle crushing on the particle contact force, the contact force was researched in the vertical and horizontal directions when the shear displacement was 0%, 10%, and 20% of the sample. The contact force rose diagrams are shown in Figs. 13 and 14. The data were analyzed in ten-degree intervals. The greater the distance from the center means the larger the contact force is. Since the contact forces are reciprocal, the rose diagram is centrosymmetric.

Figs. 13 and 14 show the same pattern. In the initial stage of the shear test, there was no particle crushing, and the contact force fabric of the particles with different strengths was the same. The normal contact force and the tangential contact force were large and both in the diagonal direction (±15° to the z-axis), and the contact force in the horizontal direction was small. As the shear test progressed, the anisotropy of the contact forces decreased. When the shear tests were completed, the projections of the contact force rose in the two directions were approximately a circle. Comparing particles with different strengths, the higher the particle strength was, the larger the contact force was, and the more obvious the anisotropy of the contact force observed. It could be found that particle crushing not only reduced the contact forces value but also reduced the anisotropy of the contact forces.

4. Discussion

The shear strength of granular materials such as gravels is derived from the friction near the shear zone, including sliding friction, rolling friction, and interlock between particles (Wei *et al*. 2021, Salazar *et al*. 2015), as shown in Fig. 15(b). The sliding friction is affected by the material and surface roughness of the particles, which is generally unchangeable. The rolling friction is determined by the external force required for particles rolling in the shear zone. The interlock refers to the gear-like engagement between nearby particles. The crushed child particles are smaller in size and can easily move and roll, reducing the rolling friction. In addition, the crushed particles in the sliding zone take up the space between large particles, which reduces the particles' moment, thereby weakening the mechanical engagement effect (Figs. 15(c) and 15(d)). Therefore, particle crushing decreases the overall shear

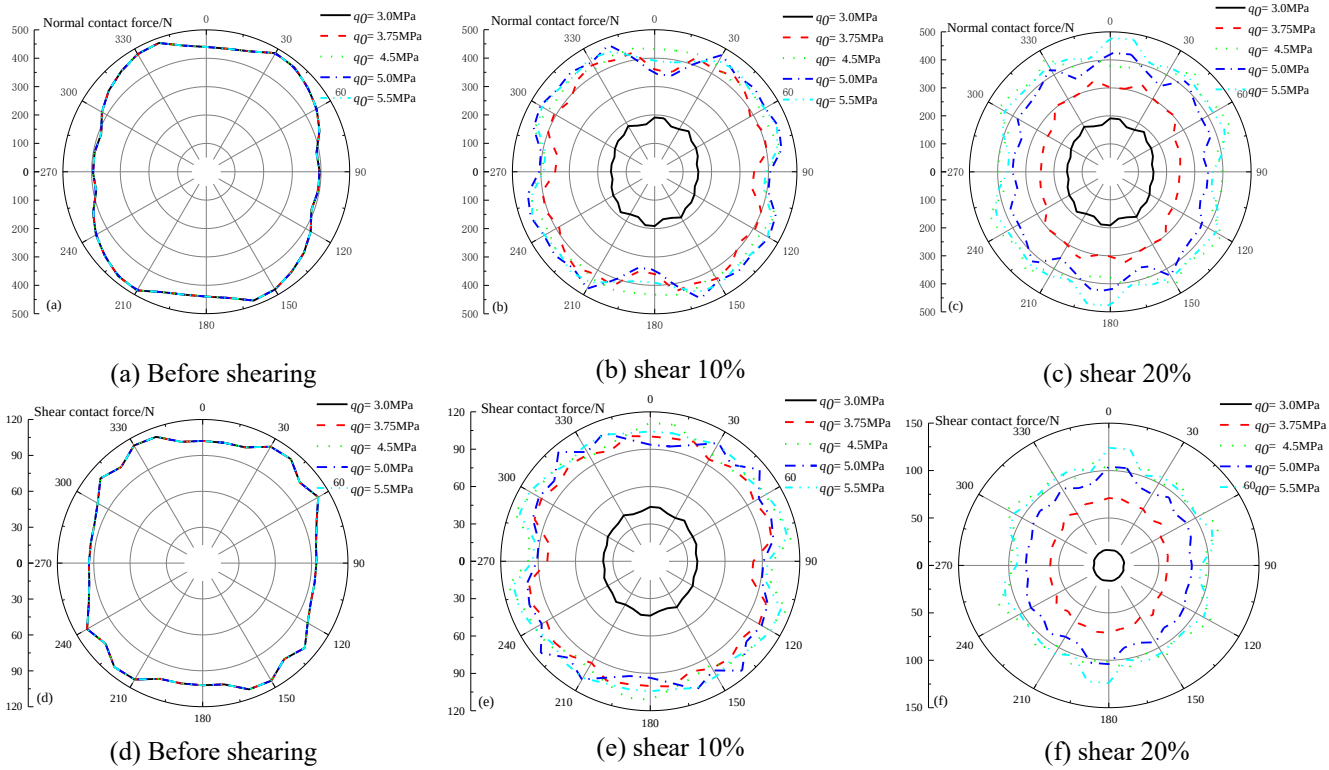

(a) Before shearing (b) shear 10% (c) shear 20%

(d) Before shearing (e) shear 10% (f) shear 20%

Fig. 13 The contact force rose in the vertical projection

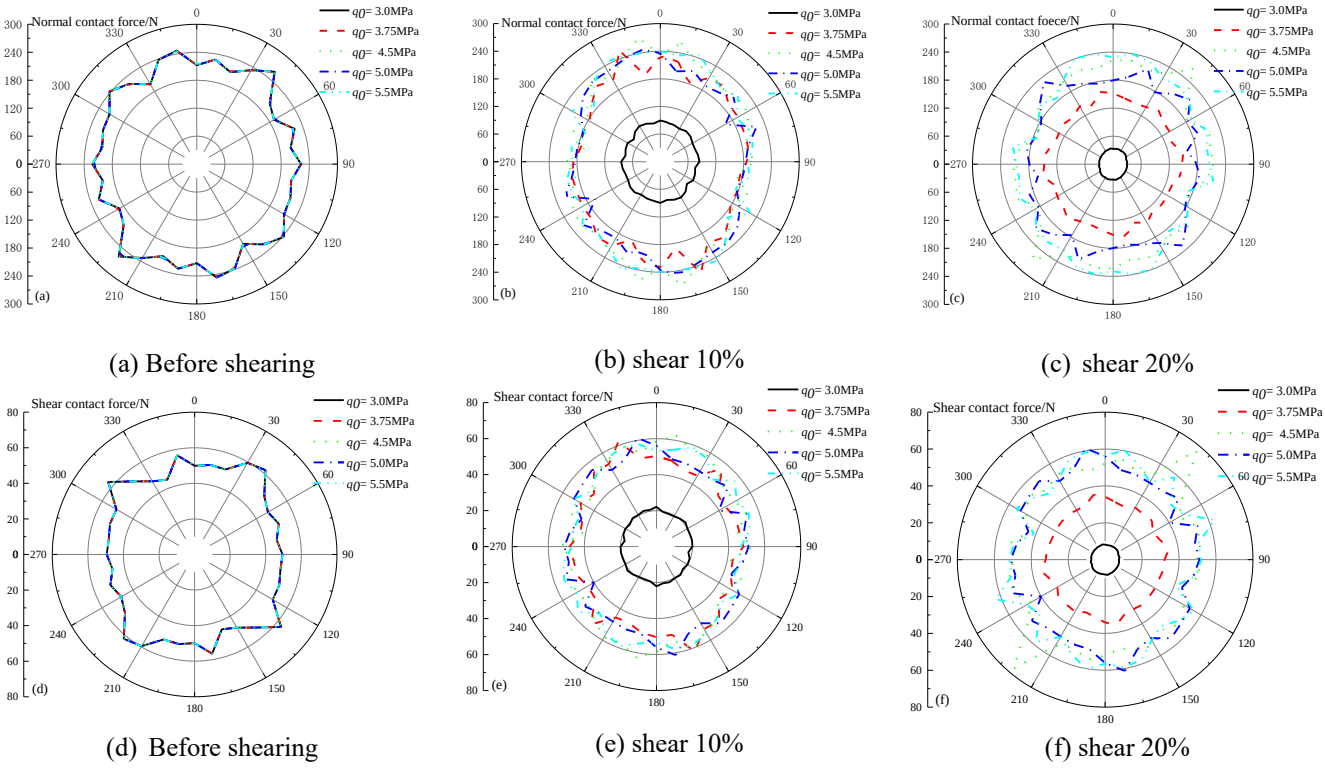

(a) Before shearing (b) shear 10% (c) shear 20%

(d) Before shearing (e) shear 10% (f) shear 20%

Fig. 14 Contact force rose in the horizon projection

strength of the material. Moreover, the shear displacement with particle crushing is the same as that at the peak shear stress, which explains why a landslide tends to develop rapidly once it occurs in gravel-filling foundations or slop.

Besides, particle crushing has an obvious effect on the shear hardening properties. When the particle crushing is limited, the static friction in the shear band becomes dynamic friction, as the shear test conducts, which presents

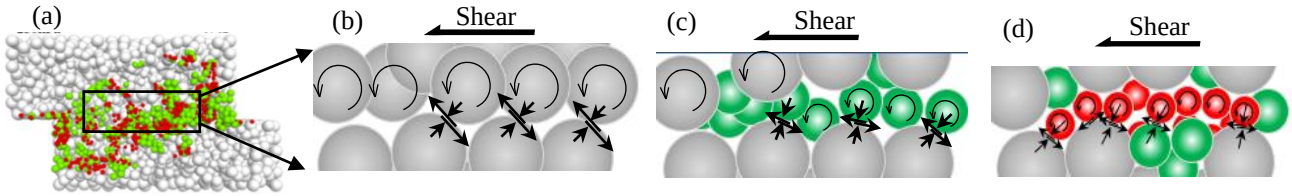

Fig. 15 Interpretation of particle crushing effect on shear strength

a sudden variation of contact force between the particles and stress redistribution (Fig. 9). Hence, peak stress occurs. As the number of crushing particles increases, the child particles reduce the friction. Hence, the peak shear stress is similar to the residual strength. When the particles further crush, the dynamic friction in the shear zone is further reduced, and the shear softening appears again.

5. Conclusions

In this study, a particle crushing model was developed based on DEM, and a series of numerical direct shear tests on gravels were carried out to study the effect of particle crushing on the shear behavior from the aspect of particle crushing evolution, displacement-shear stress, internal friction angle, volumetric strain behavior, and contact force fabric. The following conclusions were obtained:

- Based on the octahedral shear stress criterion and Apollonian sphere packing, a DEM model accounting for particle crushing was developed. This model satisfied the mass conservation, was suitable for the number of particles contact changing, and overcame the problem of local stress concentration between child particles.
- The number of crushed particles increases with the shear displacement and axial pressure increasing, and with the characteristic strength decreasing. In the shearing process, the particles underwent crushing multiple times, which were mainly located at the diagonal direction of the shear box and the shear zone.
- The particle crushing decreased the shear strength and corresponding shear displacement, the Mohr-Coulomb strength curve was no longer linear, and the starting point of particle crushing was close to the shear displacement at the peak shear stress. Besides, particle crushing has influences on shear-hardening properties, which could be explained by that particle crushing decreased the interlock and the rolling friction between particles.
- With the number of child particles increasing, the contact force rose diagram becomes circular, and the magnitude and anisotropy of the contact force between particles decrease, indicating significant shear contraction characteristics.
- Particle crushing will damage the particles' interlock and further reduce the strength and shear dilation, which may provide a novel method for stability evaluation and treatment of slopes. To improve the calculation efficiency of the model, the particle crushing process was simplified by replacing the crushed particle with four child particles. Further analysis may be carried out using the actual crushing characteristics of coarse-grained soil.

Acknowledgments

This research was supported by the National Natural Science Foundation of China (NO. 52278435, No. 51908066), the Science and Technology Talent Promotion Program of Hunan Province (No. 2023TJ-N12), and the Open Fund of National Engineering Research Center of Highway Maintenance Technology (Changsha University of Science & Technology, No. kfj210103).

References

Armaghani, D.J., Mirzaei, F., Toghroli, A. and Shariati, A. (2020), "Indirect measure of shear strength parameters of fiber-reinforced sandy soil using laboratory tests and intelligent systems", *Geomech. Eng.*, **22**(5), 397-414. https://doi.org/10.12989/gae.2020.22.5.397.

Ben-Nun, O. and Einav, I. (2008), "A refined DEM study of grain size reduction in uniaxial compression", *Proceedings of the 12th international conference of the international association for computer methods and advances in geomechanics (IACMAG)*, Goa, India, October.

Ben-Nun, O. and Einav, I. (2009), "The role of self-organization during confined comminution of granular materials", *Philosophical Transactions of the Royal Society A: Mathematical, Physical and Engineering Sciences*, **368**(1910), 231-247. https://doi.org/10.1098/rsta.2009.0205.

Borkovec, M., De Paris, W. and Peikert, R. (1994), "The fractal dimension of the Apollonian sphere packing", *Fractals*, **2**(4), 521-526. https://doi.org/10.1142/s0218348x94000739.

Chen, H., Wei, H., Meng, Q., Wang, Z. and Feng, Z. (2018), "The study on stress-strain-strength behavior of calcareous sand with particle breakage", *Eng. Geol.*, **26**(6), 1490-1498. https://doi.org/10.13544/j.cnki.jeg.2017-519.

Ciantia, M.O., Arroyo, M., Calvetti, F. and Gens, A. (2015), "An approach to enhance efficiency of DEM modelling of soils with crushable grains", *Géotechnique*, **65**(2), 91-110. https://doi.org/10.1680/geot.13.p.218.

Cundall, P.A. (1988), "Computer simulations of dense sphere assemblies", *Micromechanics of Granular Materials - Proceedings of the U.S./Japan Seminar on the Micromechanics of Granular Materials*, Sendai-Zao, Japan, October 26-30, 1987.

de De Bono, J.P. and McDowell, G.R. (2014), "DEM of triaxial tests on crushable sand", *Granular Matter.*, **16**(4), 551-562. https://doi.org/10.1007/s10035-014-0500-x.

Gong, J., Cheng, L.P., Zhao, L.H., Zou, J.F., Li, L. and Nie, Z.H. (2021), "Study on the packing and shear characteristics of granular mixtures via the DEM", *Geomech. Eng.*, **27**(3), 223-237. https://doi.org/10.12989/gae.2021.27.3.223.

Indraratna, B., Thakur, P.K. and Vinod, J.S. (2010), "Experimental and numerical study of railway ballast behavior under cyclic loading", *Int. J. Geomech.*, **10**(4), 136-144. https://doi.org/10.1061/(asce)gm.1943-5622.0000055.

Ke-fen, Z., Sheng, Z., Ji-dong, T. and Dai-chao, S. (2017), "3D numerical simulation of particle breakage using discrete element method", *Rock Soil Mech.*, **38**(7), 2119-2127. https://doi.org/10.16285/j.rsm.2017.07.036.

Kumar, S.A. and Sujatha, E.R. (2021), "Experimental investigation on the shear strength and deformation behaviour of xanthan gum and guar gum treated clayey sand", *Geomech. Eng.*, **26**(2), 101-115. https://doi.org/10.12989/gae.2021.26.2.101.

Li, X., Zhang, K., Ma, X., Teng, J. and Zhang, S. (2020), "New method to evaluate strengthen efficiency by dynamic compaction", *Int. J. Geomech.*, **20**(4), 04020024. https://doi.org/10.1061/(asce)gm.1943-5622.0001586.

Likitlersuang, S., Chheng, C., Surarak, C. and Balasubramaniam, A. (2018), "Strength and stiffness parameters of Bangkok clays for finite element analysis", *Geotech. Eng.*, **49**(2), 150-156.

Likitlersuang, S., Teachavorasinskun, S., Surarak, C., Oh, E. and Balasubramaniam, A. (2013), "Small strain stiffness and stiffness degradation curve of Bangkok Clays", *Soils Found.*, **53**(4), 498-509. https://10.1016/j.sandf.2013.06.003

Liu, Y., Gao, R. and Chen, J. (2021), "A new DEM model to simulate the abrasion behavior of irregularly-shaped coarse granular aggregates", *Granular. Matter.*, **23**(3), 1-16. https://doi.org/10.1007/s10035-021-01130-5.

Lobo-Guerrero, S. and Vallejo, L.E. (2006), "Discrete element method analysis of railtrack ballast degradation during cyclic loading", *Granular. Matter.*, **8**(3), 195-204. https://doi.org/10.1007/s10035-006-0006-2.

Ma, G., He, X., Jiang, X., Liu, H., Chu, J. and Xiao, Y. (2020), "Strength and permeability of bentonite-assisted biocemented coarse sand", *Can. Geotech. J.*, **58**(7), 969-981. https://doi.org/10.1139/cgj-2020-0045.

Mase, L.Z., Likitlersuang, S. and Tobita, T. (2019), "Cyclic behaviour and liquefaction resistance of Izumio sands in Osaka, Japan", *Mar. Georesour. Geotech.*, **37**(7), 765-774. https://doi.org/10.1080/1064119X.2018.1485793.

McDowell, G.R. and Humphreys, A. (2002), "Yielding of granular materials", *Granular. Matter.*, **4**(1), 1-8. https://doi.org/10.1007/s10035-001-0100-4.

McDowell, G.R., De Bono, J.P., Yue, P. and Yu, H.S. (2013), "Micro mechanics of isotropic normal compression", *Géotechnique Lett.*, **3**(4), 166-172. https://doi.org/10.1680/geolett.13.00050.

Russell, A.R. and Wood, D.M. (2009), "Point load tests and strength measurements for brittle spheres", *Int. J. Rock Mech. Min. Sci.*, **46**(2), 272-280. https://doi.org/10.1016/j.ijrmms.2008.04.004.

Russell, A.R., Wood, D.M. and Kikumoto, M. (2009), "Crushing of particles in idealised granular assemblies", *J. Mech. Phys. Solids*, **57**(8), 1293-1313. https://doi.org/10.1016/j.jmps.2009.04.009.

Salazar, A., Sáez, E. and Pardo, G. (2015), "Modeling the direct shear test of a coarse sand using the 3D Discrete Element Method with a rolling friction model", *Comput. Geotech.*, **67**, 83-93. https://doi.org/10.1016/j.compgeo.2015.02.017.

Shen, C., Liu, S., Wang, L. and Wang, Y. (2019), "Micromechanical modeling of particle breakage of granular materials in the framework of thermomechanics", *Acta Geotechnica*, **14**(4), 939-954. https://doi.org/10.1007/s11440-018-0692-z.

Shi, H., Zhang, H. and Song, L. (2020), "Evolution of sandstone shear strength parameters and its mesoscopic mechanism", *Geomech. Eng.*, **20**(1), 29-41. https://doi.org/10.12989/gae.2019.20.1.029.

Sukkarak, R., Likitlersuang, S., Jongpradist, P. and Jamsawang, P. (2021), "Strength and stiffness parameters for hardening soil model of rockfill materials", *Soils Found.*, **61**(6), 1597-1614. https://doi.org/10.1016/j.sandf.2021.09.007.

Sukkarak, R., Tanapalungkorn, W., Likitlersuang, S. and Ueda, K. (2021), "Liquefaction analysis of sandy soil during strong earthquake in Northern Thailand", *Soils Found.*, **61**(5), 1302-1318. https://doi.org/10.1016/j.sandf.2021.07.003.

Sun, W., Wu, S. and Xu, X. (2021), "Mechanical behaviour of Lac du Bonnet granite after high-temperature treatment using bonded-particle model and moment tensor", *Comput. Geotech.*, **135**, 104132. https://doi.org/10.1016/j.compgeo.2021.104132.

Surarak, C., Likitlersuang, S., Wanatowski, D., Balasubramaniam, A., Oh, E. and Guan, H. (2012), "Stiffness and strength parameters for hardening soil model of soft and stiff Bangkok clays", *Soils Found.*, **52**(4), 682-697. https://10.1016/j.sandf.2012.07.009.

Takei, M., Kusakabe, O and Hayashi, T. (2001), "Time-dependent behavior of crushable materials in one-dimensional compression tests", *Soils Found.*, **41**(1), 97-121. https://doi.org/10.3208/sandf.41.97.

Tavares, L.M. and Anderson, S. (2021), "A stochastic particle replacement strategy for simulating breakage in DEM", *Powder Technol.*, **377**, 222-232. https://doi.org/10.1016/j.powtec.2020.08.091.

Thay, S., Likitlersuang, S. and Pipatpongsa, T. (2013), "Monotonic and cyclic behavior of Chiang Mai sand under simple shear mode", *Geotech. Geol. Eng.*, **31**, 67-82. https://doi.org/10.1007/s10706-012-9563-9.

Tu, Y.L., Wang, X.C., Lan, Y.Z., Wang, J.B. and Liao, Q. (2022), "Mechanical properties and failure mechanism of gravelly soils in large scale direct shear test using DEM", *Geomech. Eng.*, **30**(1), 27-44. https://doi.org/10.12989/gae.2022.30.1.027.

Ueng, T.S. and Chen, T.J. (2000), "Energy aspects of particle breakage in drained shear of sands", *Géotechnique*, **50**(1), 65-72. https://doi.org/10.1680/geot.2000.50.1.65.

VandenBerge, D.R., Valentine, R.J., Brandon, T.L. and Wright, S.G. (2021), "Case history: Failure of the reinforced soil slope at Yeager Airport, Charleston, West Virginia", *J. Geotech. Geoenviron. Eng.*, **147**(1), 05020013. https://doi.org/10.1061/(asce)gt.1943-5606.0002430.

Wang, P., Yin, Z.Y. and Wang, Z.Y. (2022), "Micromechanical investigation of particle-size effect of granular materials in biaxial test with the role of particle breakage", *J. Eng. Mech.*, **148**(1), 04021133. https://doi.org/10.1061/(ASCE)EM.1943-7889.0002039.

Wei, H., Li, X., Zhang, S., Zhao, T., Yin, M. and Meng, Q. (2021), "Influence of particle breakage on drained shear strength of calcareous sands", *Int. J. Geomech.*, **21**(7), 04021118. https://doi.org/10.1061/(ASCE)GM.1943-5622.0002078.

Wei, H., Yin, M., Zhao, T., Yan, K., Shen, J., Meng, Q. and He, J. (2021), "Effect of particle breakage on the shear strength of calcareous sands", *Mar. Geophys. Res.*, **42**(3), 1-11. https://doi.org/10.1007/s11001-021-09440-2.

Xiao, Y., Chen, H., Stuedlein, A.W., Evans, T.M., Chu, J., Cheng, L. and Aboel-Naga, H.M. (2020), "Restraint of particle breakage by biotreatment method", *J. Geotech. Geoenviron. Eng.*, **146**(11), 04020123. https://doi.org/10.1061/(asce)gt.1943-5606.0002384.

Xiao, Y., Wang, C., Wu, H. and Desai, C.S. (2021), "New simple breakage index for crushable granular soils", *Int. J. Geomech.*, **21**(8), 04021136. https://doi.org/10.1007/s11001-021-09440-2.

Xu, Y.R. and Xu, Y. (2021), "Numerical simulation of direct shear test of rockfill based on particle breaking", *Acta Geotechnica*, **16**(10), 3133-3144. https://doi.org/10.1007/s11440-021-01172-2.

Xu, Z.H., Wang, W.Y., Lin, P., Xiong, Y., Liu, Z.Y. and He, S.J. (2020), "A parameter calibration method for PFC simulation: Development and a case study of limestone", *Geomech. Eng.*, **22**(1), 97-108. https://doi.org/10.12989/gae.2020.22.1.097.

Yang, Z., Cai, H., Dai, M., Wang, T. and Li, M. (2022), "Mechanical behavior and rock breaking mechanism of shield hob based on Particle Flow Code (PFC) method", *Geotech. Geol. Eng.*, 1-18. https://doi.org/10.1007/s10706-022-02286-4.

Yu, F. (2017), "Particle breakage and the drained shear behavior of sands", *Int. J. Geomech.*, **17**(8), 04017041. https://doi.org/10.1061/(ASCE)GM.1943-5622.0000919.

Zhang, K.F., Zhang, S., Teng, J.D. and Sheng, D.C. (2018), "Influences of self-organization of granular materials on particle crushing based on discrete element method", *Chinese J. Geotech. Eng.*, **40**(4), 743-751.

Zhang, R., Zhao, C., Yang, C., Xing, J. and Morita, C. (2021), "A comprehensive study of single-flawed granite hydraulically fracturing with laboratory experiments and flat-jointed bonded particle modeling", *Comput. Geotech.*, **140**, 104440. https://doi.org/10.1016/J.COMPGEO.2021.104440.

Zhou, W., Yang, L., Ma, G., Chang, X., Lai, Z. and Xu, K. (2016), "DEM analysis of the size effects on the behavior of crushable granular materials", *Granular. Matter.*, **18**(3), 1-11. https://doi.org/ 10.1007/s10035-016-0656-7.

CC